Brain tumour classification utilizing MRI images employing an auxiliary classifier based on generative adversarial networks

Prajith Prabhakar[1], Yokesh V[2], P Selvaraj[3], M Bharathi[4]

[1]Department of Thermal Engineering, Saveetha School of Engineering, Saveetha Institute of Medical and Technical Science, Chennai, India.

[2]Department of Electronics and Communication Engineering, Sathyabama Institute of Science and Technology, Chennai, India.

[3]Associate Professor, Electrical and Electronics Engineering,

Dr.M.G.R. Educational and Research Institute, Chennai, TamilNadu.

[4]Assistant professor, Department of Electronics and communication Engineering

Jeppiaar institute of technology, Sriperumbudur.

Abstract

Medical image analysis has recently seen a surge in interest in the application of AI approaches, especially for the purpose of detecting and classifying brain cancers. Using magnetic resonance imaging (MRI) scans and a U-Net-based neural network for segmentation, we have developed a novel approach to the detection and classification of brain tumors. Using MRI data, this study proposes a novel approach to identifying and categorizing brain tumors. The suggested approach accurately and efficiently segments and classifies brain cancers by combining ACGAN with a U-Net architecture. Features from magnetic resonance imaging (MRI) scans are retrieved using the U-Net architecture, and then classified using the ACGAN architecture. This research presents a new method for identifying and categorizing brain cancers in magnetic resonance imaging (MRI) scans using a U-Net-based architecture known as Auxiliary Classifier Generative Adversarial Networks (ACGAN). The proposed framework trainable on a large dataset of magnetic resonance imaging (MRI) photos that contains both tumor and non-tumor images may generate synthetic tumor images that are very comparable to real tumor images. In order to make the model better at detecting and classifying tumors, the generated photos are used. After correctly segmenting tumor regions in MRI images, the ACGAN-U-Net classifier uses a U-Net-based architecture to classify the tumors into different kinds. The experimental results reveal that the proposed model outperforms current state-of-the-art

methods in terms of sensitivity, specificity, and accuracy; this proves that ACGAN-U-Net can be used clinically for brain tumor detection and classification using U-Net.

Keywords: Hybrid deep learning, brain tumor classification, Auxiliary Classifier Generative Adversarial Networks (ACGAN), U-Net, Magnetic Resonance Imaging (MRI).

1. Introduction

Brain tumor disorders, which severely impact people and are life-threatening, have attracted a lot of attention lately. Brain cancer ranks as the tenth most common primary cause of death for both men and women. More than 126,000 people are diagnosed with brain tumors yearly, and more than 97,000 of them pass away, according to the National Institute for Research on Cancer. However, there is a wide range in the prognosis for persons with malignant brain tumors, and it depends on a number of variables, such as the patient's age and the type of the tumor. White matter (WM), grey matter (GM), and cerebral spinal fluid are the three principal components that make up normal brain tissue (CSF).

The human brain is an essential part of the human nervous system that serves as a command center for daily bodily functions. The body's sensory organs send signals or stimuli to the brain, interpreting them and then controlling the action. The brain gathers information from the body's sensory organs, analyzes it, draws conclusions, and then communicates it to the muscles. BTs, which cause an unchecked expansion of abnormal brain cells, are one of the most significant extreme circumstances affecting the human brain [1]. Primary metastatic and secondary metastatic BTs are the two distinct subtypes. The benign tumors known as primary brain tumors (BTs) progress from the cells of the human brain. The blood flow from other body portions, on the other hand, is how secondary metastatic tumors reach the brain.

The World Health Organization (WHO) also ordered BTs into four grades (Grades I–IV) based on their classification as benign or malignant. Magnetic resonance imaging (MRI) and computer tomography are the two methods greatest frequently employed to detect and evaluate BTs (CT). Malignant BTs of results III and IV rapidly invade healthy cells as they spread throughout the body. Early BT detection and organization, based on MRI and other imaging data, enables doctors to plan the best course of action [2]. Glioma, pituitary, and meningioma are the three basic brain tumor categories most frequently found. Pituitary BTs, generally benign, are produced by the pituitary glands located in the center of the brain and are accountable for making some of the body's most significant hormones.

Gliomas progress from glial cells in the brain. Meningioma cancers typically form in the membranes that cover and shield the brain and spinal cord [3]. It is essential to distinguish between normal and abnormal brain tissue to detect BT. BT detection is a persistent open problem due to size, shape, and position variations. Medical image processing concepts (like classification, segmentation, and detection) are applied in BT analysis [4]. If there is a tumor type, it must be identified early on using the BT classification procedure. In biomedical image processing, various futuristic computer-aided diagnosis systems are accessible to help radiologists guide patients and categorize BTs more accurately [5]. A BT is a risky condition that shortens life expectancy when high-grade tumors occur. To be more precise, a BT diagnosis is advantageous to the patient's life and the course of their action [6]. Due to the high variance, low contrast, and distorted edges of nasopharyngeal carcinoma magnetic resonance images (MRIs) (NPC).

Brain tumor classification techniques fall into machine learning (ML) and deep learning (DL). In ML-based systems, feature extraction and segmentation are performed manually, which is labor-intensive, sluggish, and prone to errors. These procedures often require the help of a specialist with vast knowledge to identify the most efficient feature extraction and segment procedures for accurate tumor diagnosis. Consequently, these schemes behave inconsistently while working with more extensive databases. On the other hand, DL-based approaches mechanized these processes and excel in a broad spectrum of uses, most notably medical image processing. [7-8].

In the present state, deep learning technology has caught the attention of many businesses, especially that medical imaging analysis (DL). Deep learning processes enormous volumes of unstructured data using numerous layers, each of which can gradually extract features and transfer them to the next. This gives deep learning strength and flexibility. The deep learning technique emphasizes automatically extracting attributes that describe data representations, making them unique. The ACGAN deep learning algorithm is the one that is most frequently used in the field of medical images. The ACGAN model is proficient at successfully extracting features and representations of structured data from medical images.

The current state-of-the-art deep learning (DL) has caught the attention of many industries, particularly that medical image analysis. Deep understanding uses multiple layers to process massive amounts of unstructured data, with each layer able to features extracted and pass them to the next grade. This strengthens and flexibilities deep learning. The automatic extraction of

attributes that describe data representations is a critical component of the deep learning approach, which sets it apart from other systems. The deep learning algorithm that is most frequently applied to the analysis of medical images is ACGAN. From medical images, the ACGAN model is adept at successfully extracting features and representations of structured data.

In contrast, this study suggests a new brain tumor categorization methodology founded on MRI brain images and a hybrid ACGAN method. Some of the study's accomplishments include:

- We suggest a hybrid deep learning model comprising Auxiliary Classification Generative Adversarial Networks (ACGAN) and a U-Net structure to accurately and effectively segment and classify brain malignancies.
- It delivers a hybrid deep learning algorithm that can spot brain tumors early on, speeding up action and preventing the feast of tumor substance.
- It establishes a hybrid deep learning organization technique that utilizes U-Net and ACGAN produces better outcomes and higher accuracy when compared to standard methods.
- Because no invasive procedures are required, it assists radiologists in avoiding errors when manually identifying malignancies from MRI pictures.

The respite of the text is structured as surveys: The second module examines connected research. Unit 3 introduces the proposed technique, Section 4 reports on experiments and discussions, and Section 5 summarizes the findings.

2. Literature Survey

Mehrotra et al. [9] employed a deep learning-based transfer learning algorithm to categorize 696 T1-weighted MRI images of brain tumors as malignant or benign. The categorization analysis used the most well-known CNN models, comprising ResNet-101, ResNet-50, GoogleNet, AlexNet, and SqueezeNet. They attained the highest accuracy of 99.04% thanks to transfer learning and an AlexNet simulation that had been trained.

The categorization analysis used the most well-known CNN models, comprising ResNet-101, ResNet-50, GoogleNet, AlexNet, and SqueezeNet. They accomplished the highest accuracy of 99.04% thanks to transfer learning and an AlexNet simulation that had been trained. Khan et al. [11] projected a deep-learning approach for categorizing brain tumors as cancerous or non-cancerous using 253 actual brain MRIs and information augmentation. Before features were

obtained using a straightforward CNN model, edge detection was performed to pinpoint the destination in an MRI image. They were 89% accurate in categorizing.

DCNet capsule algorithms networks and diverse capsule networks were made by Phaye et al. [12]. In essence, DCNet is a more complex convolutional network that enables learning unique feature maps. DCNet is more effective at understanding complex data because it uses a hierarchical learning architecture. Only data from three different types of brain cancers were utilized to classify a dataset of 3064 Image data from 233 brain tumor patients; healthy persons were not considered. The original convolutional layers were reduced to four layers with 16 kernels to generate the DCNet model, which was then trained using eightfold cross-validation. While the algorithm being tested had an accuracy of 93.04%, the DCNet algorithm had an accuracy of 95.03%.

Abd-Ellah and others [13] A two-phase, multi-model automated brain tumor diagnosis method based on magnetic resonance images use convolutional neural networks. CNNs were used to find brain tumors on images from magnetic resonance imaging automatically. The impartial of this study was to distinguish between images of brain tumors and images of healthy brains. A multi-model, two different systems were employed to make the diagnosis. A CNN was employed in the first stage for feature selection and pre-processing, and an error-correcting productions SVM was used in the second phase for classification (ECOC-SVM). Three methods—VGG-16 and VGG-19—were used in the early phase; AlexNet delivered the best results (99.55% accuracy). In the initial stage of the investigation, photos from the well-known reference image database RIDER neuro MRI were used to identify brain tumors while the function was being measured.

Deep learning methods were working by Paul et al. [14] to categorize images of the brain connected to meningioma, glioma, and pituitary cancers. This study used 3064 T1-weighted, especially in comparison to MRI brain pictures from 233 patients, to construct secured and CNN neural networks. With an accuracy of 91.43%, a fivefold cross-validation analysis demonstrates that the general procedures beat the particular approaches, which necessary picture dilation.

An automated method was created by Gumaei et al. [15] to help radiologists and doctors recognize different kinds of brain tumors. The three stages of the research were preprocessing of brain images, feature extraction from the brain, and classification of brain tumors. Brain images were converted into intensity pictures of the brain in the [0, 1] domain during the

preprocessing stage using a min-max normed. Subsequently, traits from MRI images were retrieved using the PCA-NGIST approach, which combines PCA and the normalization GIST descriptor. The various tumor kinds were discovered and categorized using Regularized Extreme Learning Machine (RELM) classifications in the last phase. For their study, Cheng's team divided the 3064 MRI images from 233 individuals into two groupings, utilizing 70% for testing and 30% for classifiers. Five different techniques were used for cross-validation. Accuracy was reported at 94.23%. However, one study limitation is the lack of a comparison with other methods.

By combining the new Growing CNN and the Stationary Wavelet Transform (SWT), Mittal et al. [16] automated the segmentation process (GCNN). These efficient techniques were applied to MRI scans to find brain cancers. According to the evaluation's findings, the suggested approach performs better than evolutionary computation, K-NN, SVM, and CNN.

Raja [17] used several methods, such as information-theoretic measurements, a hybrid DAE technique, wavelet packet Tsallis entropy, Bayesian fuzzy clustering (BFC) for image segmentation, a nonlocal mean filter for image denoising and scattering transform, and Bayesian imprecise measurement. However, this approach could be more computationally efficient and time-consuming. According to Afshar et al. [18], Capsule Networks were 90.89% accurate at recognizing and categorizing brain lesions. CapsNets perform best when trained on image sequences because they are susceptible to image backgrounds. As a result, understanding the architecture takes time and effort.

Ari et al. [19] combined the deep features of AlexNet and VGG16. An extreme learning machine (ELM) was used to categorize the fused feature vector. MRI images from freely accessible datasets like Figshare, Rider, and REMBRANDT were used in the study. The system's accuracy was 96.6%. Using the entire volumetric T1-Gado MRI sequence from the Brats 2018 dataset, Mzoughi et al. [20] demonstrated 3D CNN architecture for categorizing glioma brain tumors into low-grade gliomas (LGG) and high-grade gliomas (HGG). Based on a 3D convolutional layer and a deep network, the technique used small kernels to mix local and global context data with reduced weights. The system had an accuracy of 96.49 %. Glioma, meningioma, and pituitary tumors were categorized by Bada and Barjaktarovic [21] using a CNN. This study used a classification block, hidden units, two "A" blocks, two "B" blocks, an input image, and one of the 22 network design layers. The network's performance was evaluated using K-fold cross-validation. The tenfold cross-validation method used in the initial

investigation produced the highest benefit of 96.56%. 3064 T1-weighted primary imaging MRI pictures from General Hospital and Tianjin, China's Nanfang Hospital, and Medical University made up the image dataset for this study.

The three CNNs that Rehman et al. [22] looked at were AlexNet, GoogleLeNet, and VGGNet. The three primary forms of brain tumors that could be recognized using deep learning methods and MRI image dispensation were meningioma, glioma, and pituitary tumors. In the last phase, auto-mated characteristics were categorized using a linear classifier. The sample size was raised while the probability of over-fitting was decreased using data augmentation techniques. The evaluation's findings revealed that, when contrasted to the other approaches, the VGG16 method had the maximum accuracy (98.69%).

Meningioma, glioma, and pituitary tumor detection techniques were developed by Pashaei et al. [23]. They used a CNN to identify topographies in imageries and reveal hidden elements from them. The proposed model comprises one fully connected layer, four pooling layers, four batch normalization, and four convolutional layers. The model developed by the authors had ten epochs, each with 16 iterations and a learning rate of 0.01. It has ten generations as well. This study also made use of the data that Cheng gave. The efficiency of the recommended perfect was assessed using a tenfold testing data technique, with 70% and 30% of the information used for system training and testing, accordingly. When the study evaluated the projected approach against MLP, Stacking, XGBoost, SVM, and RBF, it was shown to be incredibly accurate (93.68%).

3. Proposed system

The suggested strategy is described in this section. Three steps make up our approach:

(a) pre-processing of brain images,
(b) brain feature extraction and
(c) classification of brain tumors,

The procedure uses a series of brain scans as input and outputs a diagnosis of the precise type of brain tumor. The projected approach's architecture is displayed in Figure 1. The following subsections provide more information on the specifics of the processes in our proposed technique.

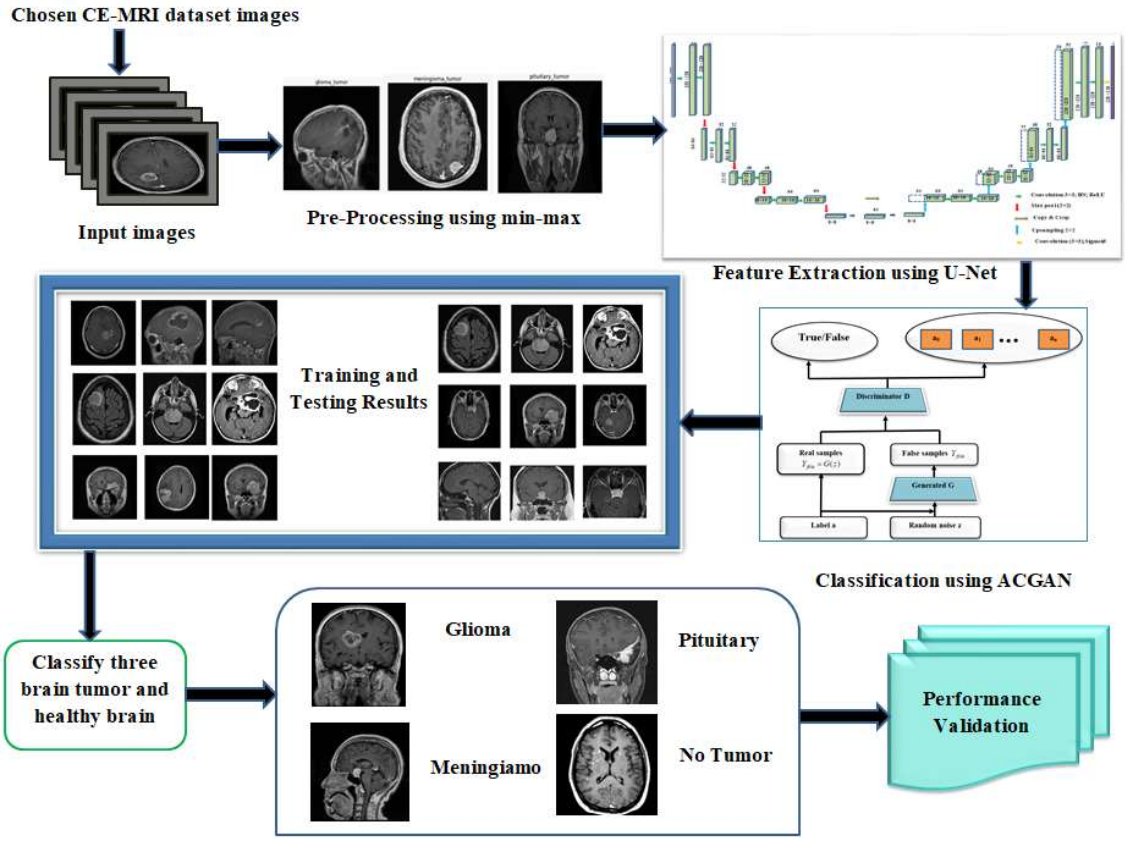

Figure 1: Proposed method of ACGAN-U-Net method

3.1 Data Collection

An available public CE-MRI dataset [24] was used in this study. The dataset includes the MRI scans of the 233 patients who underwent BTs at the General Hospital of Tianjin Medical University and the Nanfang Hospital in Guangzhou, China, over five years (2005–2010). The 3064 MRI pictures from three different angles reflect the 233 patients with three different types of BT, including gliomas (1426), meningiomas (708), and pituitary tumors (930). The specifics of the research data collection are described in full in Table 1 and Figures 2(a), 2(b), and 2(c).

Table 1: MRI-CE Dataset

Type of tumor	Patient count	No MRI pictures
Gliomas	89	1426
Pituitary	62	930
Meningioma	82	708
Entire number of images		3064

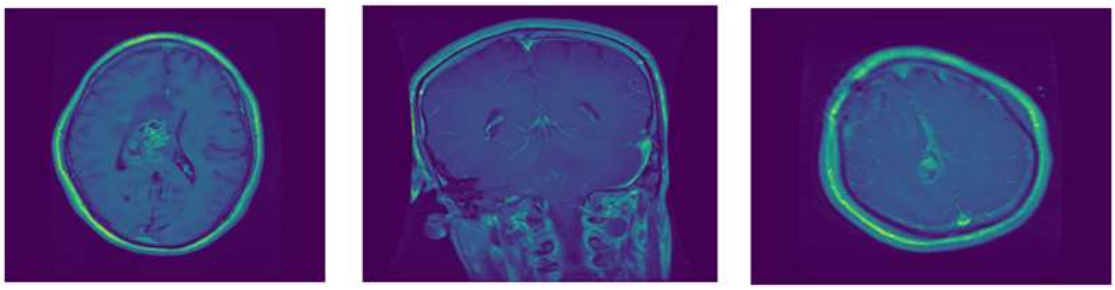

Figure 2(a): Gliomas sample images

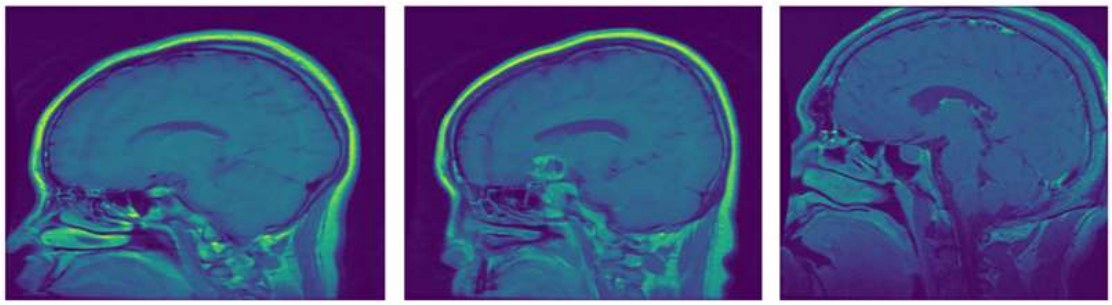

Figure 2(b): Pituitary sample images

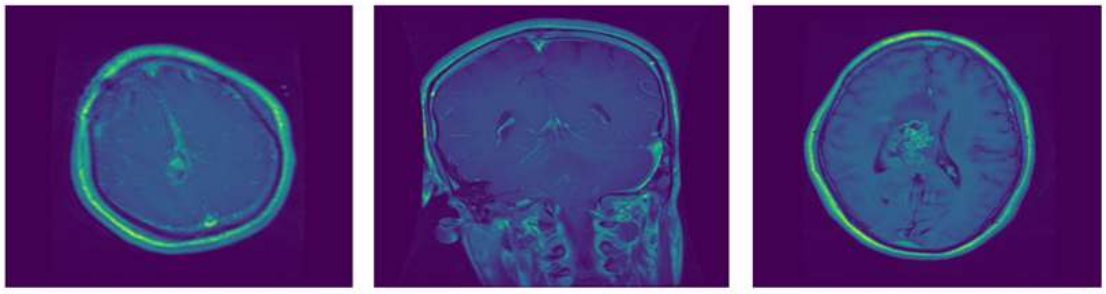

Figure 2(c): Meningioma sample images

3.2 Pre-processing

Pre-processing of brain pictures considerably improves the precision of brain feature extraction and the outcomes of brain analysis. When the input brain images were evaluated, it was found that they had significant values, including negative values, outside of the [0, 255] range. As a result, using a min-max normalizing rule and the equation below, the brain images are transformed in this stage of our method into amplitude brain images in the [0, 1] range. Figure 3 displays the pre-processing of MRI brain images.

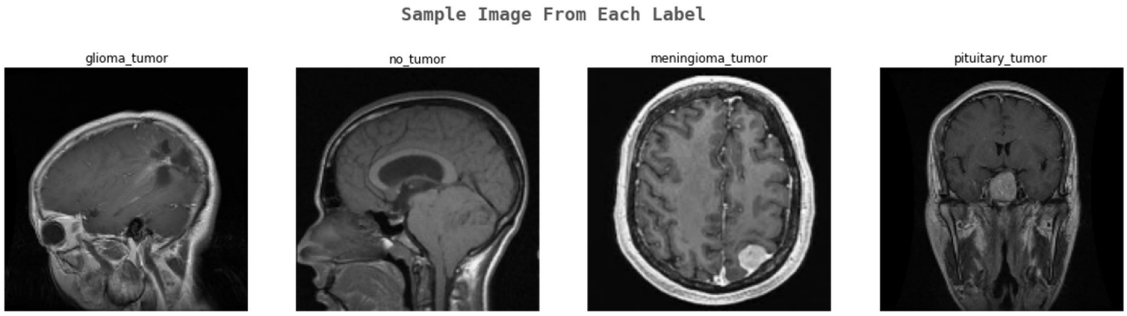

Figure 3: processing in preparation of brain images

$$f(y,z) = \frac{f(y,z) - B_{\min}}{B_{\max} - B_{\min}} \quad (1)$$

f represents the brain, and Bmin and Bmax are the image's minimum and maximum values, respectively (f). As a result, the borders and regions of the brain will have improved contrast.

3.3 Feature Extraction

Images are successfully segmented into semantically related parts using U-Net, a fully linked CNN. This U-Net deep neural network is suitable for many analytical tasks and has many applications. The autoencoder network, which converts inputs to outputs, is the cornerstone of the U-Net architecture. An auto-encoder network functions as a latent-space demonstration, effectively a compacted presentation of the images by determining the data sets most equally spaced from one another. After that, the output is created using the rebuilt compressed data [25]. Pathways for encoders and decoders are present in an autoencoder network. The encoder alters the input information into a latent-space form, which the decoder subsequently uses to reconstruct the original data. Convolutional layers are used to encrypt and decrypt the contribution images in the autoencoder design of the U-convolutional Net.

U-Net has two paths, which resemble those of an autoencoder network: an expanding symmetric expanding path and a contracting encoder path (decoder). The U-Net encoder path, just a combination of convolutional and pooling layers, captures the context of the contribution image. The decoder path employs transposed convolutions for accurate localization. The U-Net only uses a layering of convolutional layers and max-pooling layers instead of a fully linked feedforward layer (or dense layer). The U-original Net design required 572×572 images, but it may be readily changed to work with any data input. As seen in Figure 4, the network may obtain more specific properties from the compressed input images by stacking numerous convolutional layers.

The input picture's dimensions must coincide with the associated map for U-Net to work. In other terms, if there is a shape in the input image, there must also be a shape in the binary bitmask (512, 512). To fit inside a receptive space model, the idea is compressed. The decoder will give you the compressed image's original format (512, 512). The image quality has a direct impact on how well U-input Networks. A backup strategy should be in place in case the first one fails. U-Net first outscored a sliding-window convolutional network in the EM segmentation task and delivered the lowest warping error afterward. Later iterations of U-ability Net improved its ability to segment images.

U-Net++, a relatively recent addition, altered the U-Net architecture with several nested dense skip routes. The network's pathways (encoder and decoder) are connected to these pathways via feature maps [26]. It was also suggested that U-Net++ function under strict regulation. The conventional output layers and intermediate levels are now used to calculate the loss. This helps resolve the gradients disappearing during loss backpropagation problems [27].

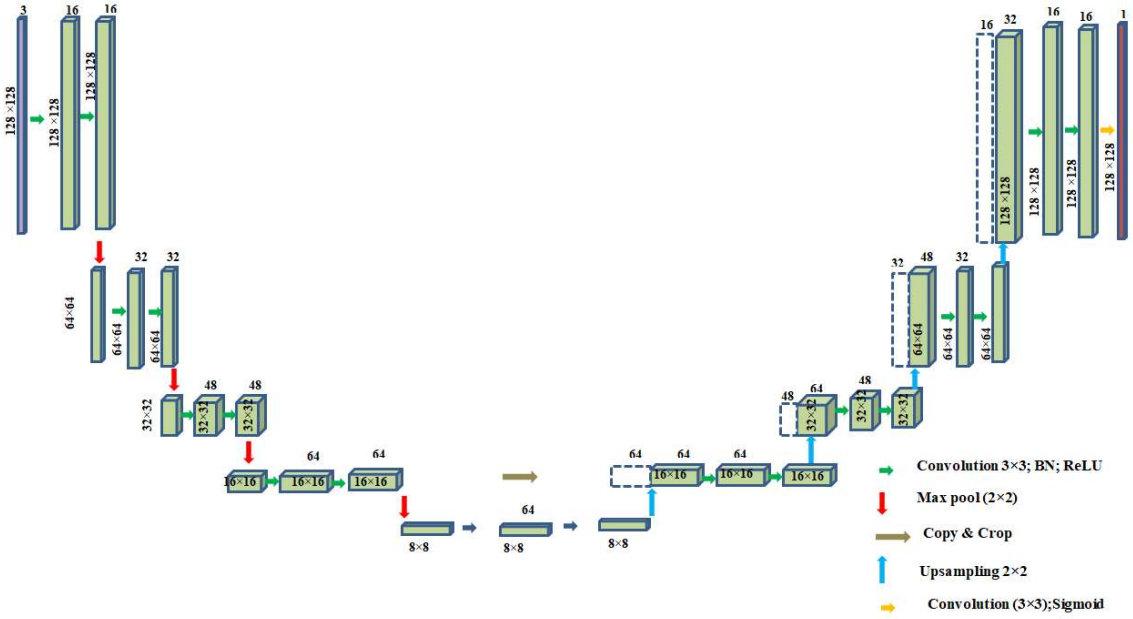

Figure 4: U-Net architecture

Because U-Net only supports two-dimensional data, the generated dataset has to be transformed from a three-dimensional picture plane using a "slice extractor" to a new dataset. The extractor extracts (stores as an MNC image) and saves each slice of an MRI scan as a PNG file.

Tensorflow 6 was used to implement the network's U-Net's convolutional blocks following the plan. The network's convolutional block comprises two layers, each with a 3×3 kernel size and zero padding, to control how much the object size shrinks after filters are applied. The filter size rises by 16 steps with each layer, while the block size for each convolutional block varies. A convolutional block is used to apply a batch normalizing step between each layer. A ReLU activates the layer. We use a 2×2 max pooling layer to further decrease the spatial dimensions of the input image, following the goal of introducing a convolutional block to the network's encoder layer. The decoder layer also makes use of max pooling. It is applied here. Use the max-pooling indexes you have learned to sample the feature map.

3.5 Classification

Conditional generative adversarial networks and semi-supervised learning with generative adversarial networks are two things of the deep learning paradigm known as GAN. While SGAN enhances the value of information created by replicating data, CGAN enhances the value created by including tag information. ACGAN broadens its benefits and gives the system a category categorization network based on these two networks.

3.5.1 Structure of ACGAN

The GAN architecture with the SVM algorithm enhances the ACGAN. ACGAN and GAN differ due to the additional training's added label information. According to Figure 5, ACGAN, which consists of a producer and a discriminator, generates finding data regarding data categories and whether the information is accurate or incorrect. Compared to other kinds of GAN models, ACGAN better considers sample variety.

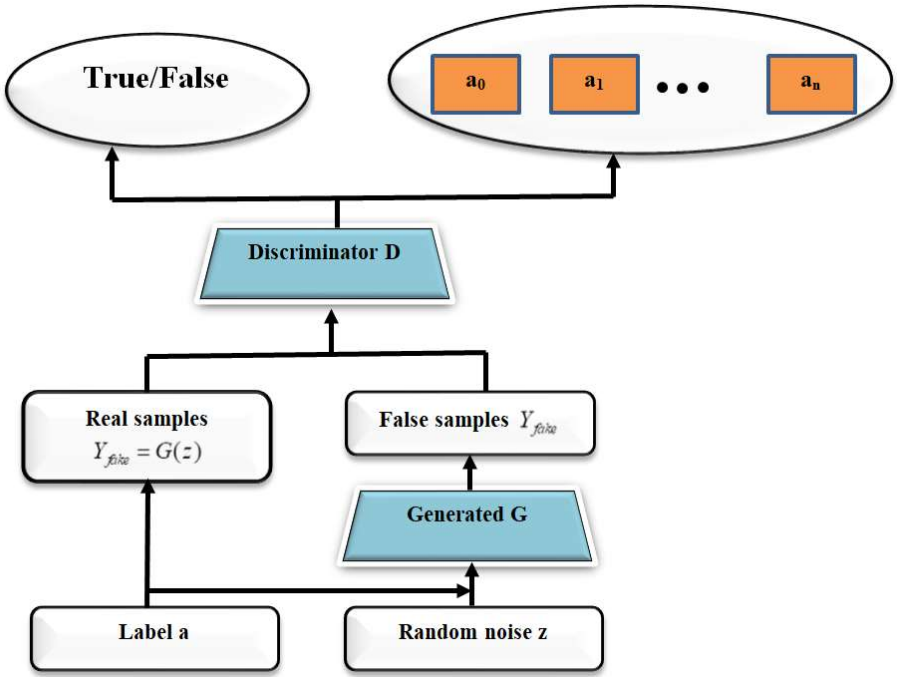

Figure 5: Structure of ACGAN

The quality of the samples produced by ACGAN can be improved by adding more categorization tags. The letter "a" in Figure 5 signifies the associated data's class label. Equations (2) and (3) show the two parts of the loss function of AGAN, respectively.

$$C_d = E_{y\sim P_{data}}\left[\log D(y)\right] + E_{z\sim P_z}\left[\log\left(1-D\left(G(z)\right)\right)\right] \tag{2}$$

$$C_a = E_{C\sim P_{data}}\left[\log D(a)\right] + E_{a\sim P_Z}\left[\log\left(1-D\left(G(a)\right)\right)\right] \tag{3}$$

The total purpose for information authenticity is represented by C_d in the calculations above, and the total purpose for information organization accuracy is represented by C_a. $y/a \sim P_{data}$ assures that Y/c follows the innovative information distribution, $z/c \sim P_z$ confirms that Y/c follows the Gaussian distribution, and z signifies chance noise. E stands for the procedure to get the mathematical expectation. Because the discriminator must be able to tell created information from accurate information as clearly as possible to categorize the data efficiently, discriminator D's training goal is to maximize $C_d + C_a$. The objective of producer G preparation is to increase $C_d - C_a$ as much as likely because it is expected that the

discriminator will effectively classify the information produced by the generator and recognize it as factual information.

3.5.2 Training Process of ACGAN

The GAN and ACGAN training processes are similar. The classifier and generator are trained alternately to generate an appropriate end optimization impact on MRI images based on the concept of zero-sum games. Actual MRI data and fictitious information recorded by the ACGAN model must be used to train the discriminator initially. After discriminator training is complete, the discriminator's settings may be temporarily left alone. Only the generator's parameters will now change in response to the discriminator's loss of feedback at this time. The generator will create fictitious data whose distribution resembles actual MRI data. The classification model will then be trained using the new fake and accurate data, which the updated generator will produce. Like before, repetition training is being conducted.

The precise training methods are: Make false MRI data G by feeding generator G a completely random noise vector with a Gaussian normal distribution (z).

Assign the category label c to the false data generated by generator G, $Y_{fake} = G(z)$, and mark it as 0. Along with the actual data, Y_{real}, as well as the category label c, one marking is appended. After batch processing both actual and fake MRI data into discriminator D simultaneously, the network terminal uses the softmax classifier to produce the distinguishing production. The following describes the improved discriminator's objective function:

$$C_D = \log H_{real} + \log(1 - H_{fake}) + \log M_{real} + \log M_{fake} \tag{4}$$

The categorization probability of the multiclassification output is H_{real} when real information are fed into the discriminator, while it is H_{fake} when false information is fed into the discriminator. When the discriminator receives incorrect data, the fake/ real (1/0) binary production is M_{real}, when false information is fed into the discriminator. When the discriminator receives incorrect data, the fake/ real (1/0) binary production M_{fake} .

Maintain the discriminator D's limitations, feed the generator G with the chance noise vector z to produce the fake information $Y_{fake} = G(z)$, and affix the associated group label c. Real and fake information is given the same label of 1, and D is the discriminator. It signifies that the

fake data Y_{fake} it failed to trick discriminator D when it was determined by discriminator D as false (the product label is 0). Maximizing the objective function

C_G of the generator is necessary to effectively fool discriminator D with the false information produced by producer G. The following is an example of how C_G is defined.

$$C_G = \log M_{fake} + \log H_{real} + \log H_{fake} \tag{5}$$

Steps 1-3 must be performed using the discriminator D and generator G after Nash equilibrium is attained, which occurs when the original and fake resolution of the discriminator D is 50%. As it closely matches how the original data disperses, the training discriminator can be used for defect discovery and classification [28].

4. Result and Discussion

The suggested Auxiliary Classifier Generative Adversarial Networks and U-Net representations were used to classify the CEMRI dataset, with 30% of the dataset being used for testing and 70% for pre-trained deep learning representations. The MATLAB environment and an i5 processor with 32 GB of RAM were used to achieve the results. There are several ways to assess how well deep learning networks perform classification tasks. F1 score, RMSE, sensitivity, specificity, accuracy, and precision were considered the most desired and preferred measures.

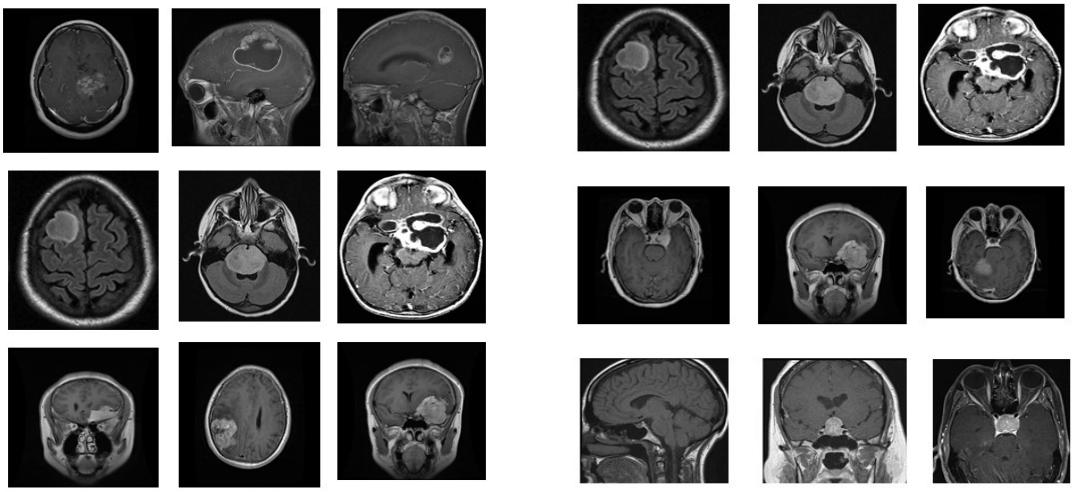

Figure 6: Training and Testing Images

4.1. Evaluation Metrics

The performance and constraints of the algorithm have been examined by analyzing the outcomes of the suggested method using the evaluation metrics listed below: As can be seen in Table 2, the confusion matrix has been applied to understand the classification performance of the model and create additional metrics that can reveal bias and algorithmic constraints.

Table 2: Matrix of Typical Confusion

	Positive	**Negative**
Positive	True Positive	False Negative
Negative	False Positive	True Negative

A classifier's prediction accuracy is evaluated. It denotes the classifier's overall performance. The precision is described as

$$Accuracy = \frac{TP + TN}{TP + FN + FP + TN} \tag{6}$$

Precision is the proportion of accurately predicted observations to all expected positive statements. High precision is associated with a low False Positive Recall.

$$\Pr ecision = \frac{TP}{TP + FP} \tag{7}$$

Another useful evaluation metric is recall, representing the proportion of correctly classified positives. The TP and FP values are used to calculate recall.

$$Sensitivity = \mathrm{Re}\,call = \frac{TP}{TP + FN} \tag{8}$$

The F1-score is calculated as the weighted average of precision and recall. It works as a numerical metric to assess the classifier's efficacy. Hence, false positives and negatives are considered while calculating this score.

$$F - Score = 2 * \frac{precision * recall}{precision + recall} \tag{9}$$

$$Specificity = \frac{TN}{FP + TN} \tag{10}$$

The Root Mean Squared Error provides the square root of the average error among actual and anticipated data (RMSE). The equation makes it possible to calculate its value (11).

$$RMSE = \sqrt{\frac{1}{n}\sum_{i=1}^{n}\left(x_i - x'_i\right)^2} \tag{11}$$

Where the forecast sample number is n; the value speed at the time i is xi; the forecasted value at period i is x I'; and the actual value at period i is the average of xi.

4.1.1. Precision Analysis

Table 3: Precision analysis for the ACGAN-Unet method using an existing system.

Number of data from Dataset	BFC	SWT-GCNN	DC-Net	RELM	ECOC-SVM	ACGAN-U-Net
100	74.76	91.54	77.87	92.88	84.56	95.98
200	75.12	91.23	80.34	93.45	85.12	95.13
300	76.34	92.17	81.34	94.19	86.77	96.24
400	77.98	92.76	82.19	94.22	88.23	97.43
500	76.12	93.18	82.54	91.67	90.87	97.12
600	75.43	94.32	83.12	92.98	90.12	97.96

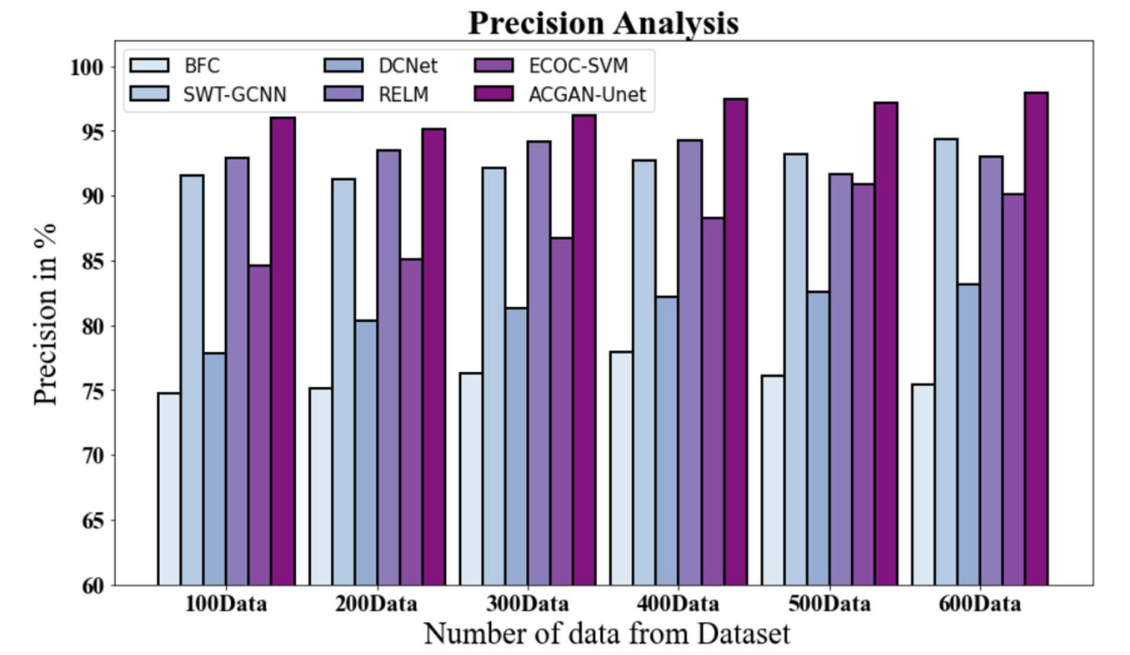

Figure 7: precision Analysis for ACGAN-Unet method with existing system

Figure 7 and Tab. 3 display a precision comparison between the ACGAN-Unet strategy and other current methodologies. The graph illustrates how performance with precision has

increased due to the machine learning approach. ACGAN-U-Net, for instance, has a precision of 95.98% concerning 100 data, while the precisions of the BFC, SWT-GCNN, DC-Net, RELM and ECOC-SVM models are, respectively, 74.76%, 91.54%, 77.87%, 92.88%, and 84.56%. However, the ACGAN-U-Net model has performed best with varying data sizes. Similarly, under 600 data points, ACGAN-U-Net has a precision of 97.96%, while BFC, SWT-GCNN, DC-Net, RELM, and ECOC-SVM have precision values of 75.43%, 94.32%, 83.12%, 92.98%, and 90.12%, respectively.

4.1.2. Sensitivity Analysis

Table 4: Sensitivity analysis for the ACGAN-U-Net method using an existing system.

Number of data from Dataset	BFC	SWT-GCNN	DC-Net	RELM	ECOC-SVM	ACGAN-U-Net
100	69.87	77.87	73.45	85.66	82.19	92.19
200	70.87	78.13	74.19	86.19	81.85	93.44
300	68.13	76.45	73.19	86.12	83.44	94.19
400	67.19	79.34	75.98	86.78	83.76	93.56
500	71.76	80.76	76.66	87.98	84.67	94.98
600	72.98	81.38	76.19	90.65	84.19	95.11

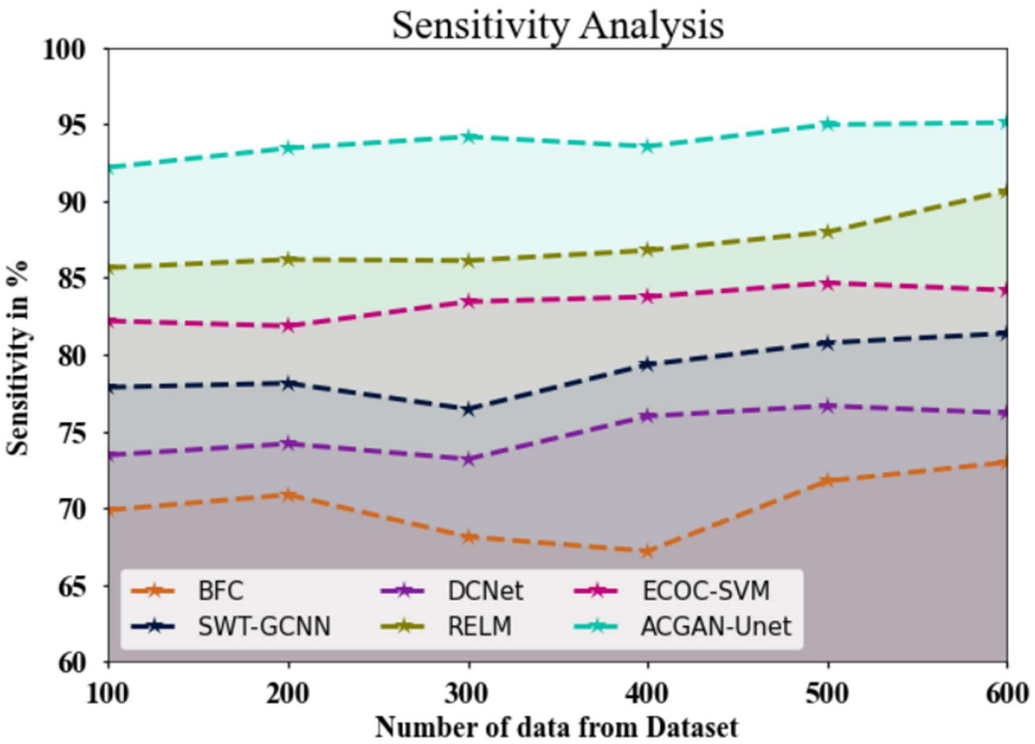

Figure 8: Sensitivity Analysis for ACGAN-U-Net method with existing system

Figure 8 and Tab.4 display a sensitivity comparison of the ACGAN-U-Net approach and other widely used techniques. The graph demonstrates that performance with sensitivity has been enhanced with the machine learning approach. ACGAN-U-Net, for instance, has a sensitivity value of 92.19% for 100 data, compared to values of 69.87%, 77.87%, 73.45%, 85.66%, and 82.19% for the BFC, SWT-GCNN, DC-Net, RELM, and ECOC-SVM models respectively. However, the ACGAN-U-Net model performed best with varying data sizes. Similarly, the ACGAN-U-Net model's sensitivity value under 600 data is 95.11%, while the BFC, SWT-GCNN, DC-Net, RELM, and ECOC-SVM models have sensitivity of 72.98%, 81.38%, 76.19%, 90.65%, and 84.19%, respectively.

4.1.3. Specificity Analysis

Table 5: ACGAN-Unet method specificity analysis with the existing system

Number of data from Dataset	BFC	SWT-GCNN	DC-Net	RELM	ECOC-SVM	ACGAN-U-Net
100	64.99	76.45	70.45	85.56	80.56	90.57
200	65.12	77.34	71.34	86.23	81.34	91.34
300	66.34	77.98	71.87	87.45	81.45	91.87
400	67.23	77.12	72.34	87.12	82.76	92.45
500	68.23	78.56	73.44	88.45	83.87	93.67
600	69.21	79.32	75.12	89.33	84.12	94.98

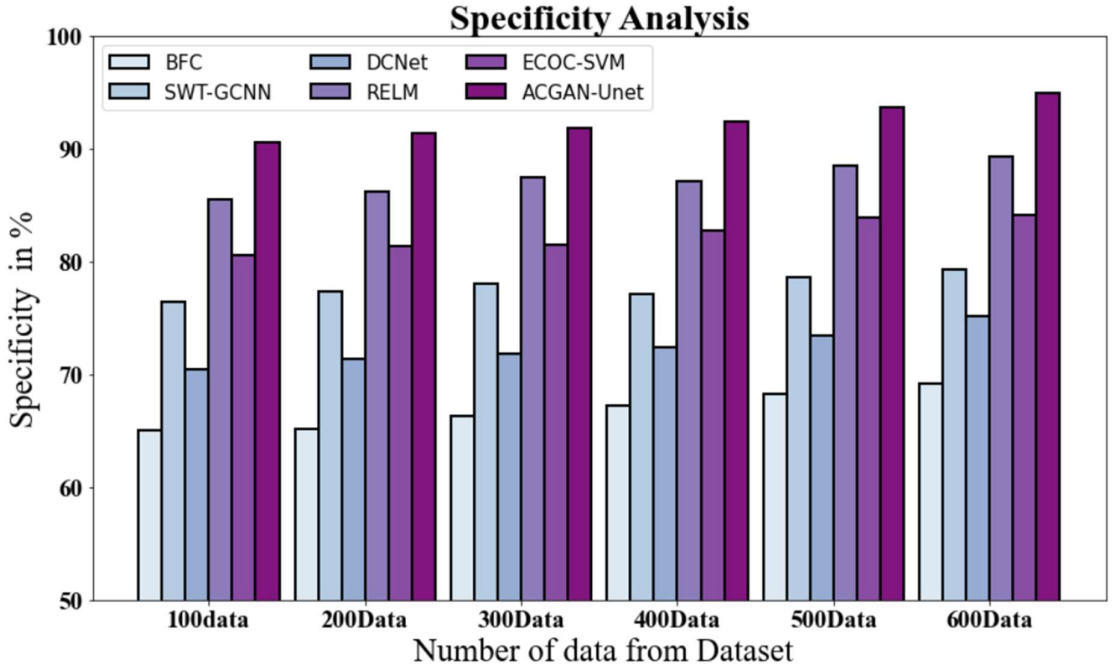

Figure 9: Specificity Analysis for ACGAN-Unet method with existing system

A specificity comparison of the ACGAN-Unet strategy with other available methods is shown in Figure 9 and Tab.5. The graph demonstrates that the specificity performance was improved using machine learning. For instance, ACGAN-Unet has a specificity of 90.57% for 100 data, compared to specificities of 64.99%, 76.45%, 70.45%, 85.56%, and 80.56% for the BFC, SWT-GCNN, DCNet, RELM, and ECOC-SVM models respectively. However, the ACGAN-Unet model performed best with varying data sizes. Similarly, under 600 data, ACGAN-Unet has a specificity of 94.98%, while BFC, SWT-GCNN, DCNet, RELM, and ECOC-SVM have specificities of 69.21%, 79.32%, 75.12%, 89.33%, and 84.12%, respectively.

4.1.4. F-Measure Analysis

Table 6: F-Measure Analysis for the ACGAN-Unet method using an existing system.

Number of data from Dataset	BFC	SWT-GCNN	DCNet	RELM	ECOC-SVM	ACGAN-Unet
100	71.89	80.76	78.12	89.98	84.12	93.87
200	72.76	81.34	79.54	89.12	84.56	94.19
300	73.19	81.23	76.12	90.65	85.12	95.67
400	75.87	82.87	77.23	91.34	85.66	97.45
500	76.11	82.65	78.54	91.45	86.78	96.11
600	77.34	83.87	79.56	92.56	88.34	97.43

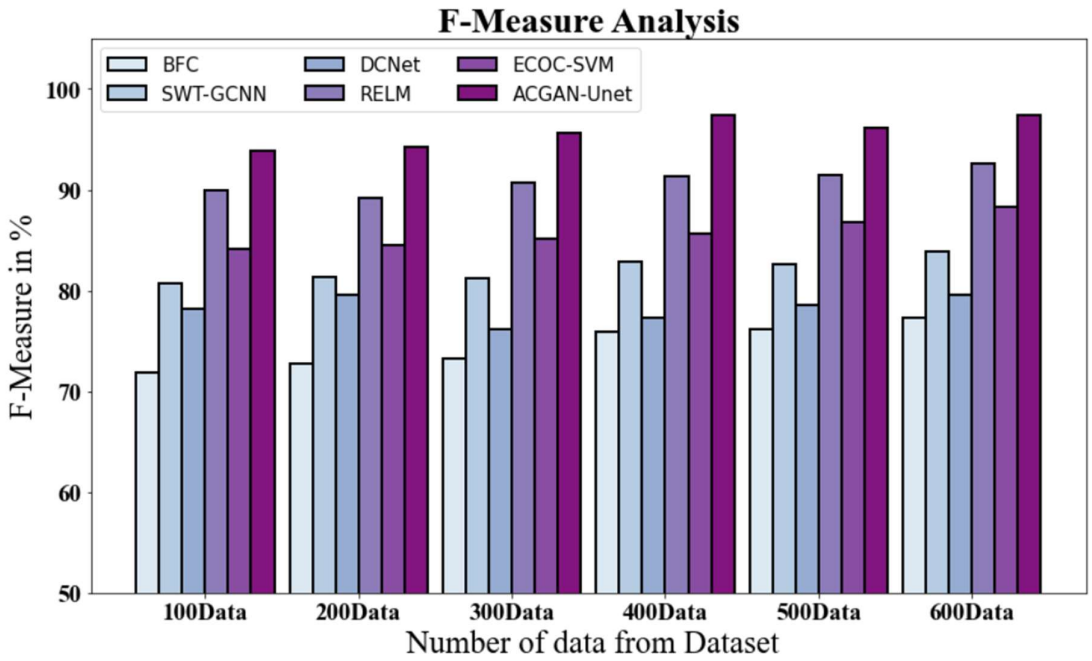

Figure 10: F-Measure Analysis for ACGAN-Unet method with existing system

Figure 10 and Tab.6 display an f-measure evaluation of the ACGAN-Unet technique and other widely used methodologies. The graph shows how the machine learning strategy has enhanced the efficiency of the f-measure. ACGAN-Unet, for instance, has a f-score value of 93.87% for

100 data, while the f-measures for the BFC, SWT-GCNN, DCNet, RELM and ECOC-SVM models have 71.89%, 80.76%, 78.12%, 89.98%, and 84.12%, respectively. However, the ACGAN-Unet model performed best with varying data sizes. Similarly, under 600 data, ACGAN-Unet has an f-measure value of 97.43%, while BFC, SWT-GCNN, DCNet, RELM, and ECOC-SVM have discounts of 77.34%, 83.87%, 79.56%, 92.56%, and 88.34%, respectively.

4.1.5. Accuracy Analysis

Table 7: Accuracy Analysis for ACGAN-Unet method with the existing system

Number of data from Dataset	BFC	SWT-GCNN	DCNet	RELM	ECOC-SVM	ACGAN-Unet
100	80.345	87.324	84.987	89.141	91.456	94.765
200	81.234	87.651	85.123	89.425	91.223	95.119
300	81.556	88.324	85.654	90.928	91.567	96.456
400	82.198	87.972	86.234	89.345	92.345	97.554
500	83.987	88.527	87.443	89.113	92.987	98.123
600	83.882	88.928	88.991	90.564	93.546	99.996

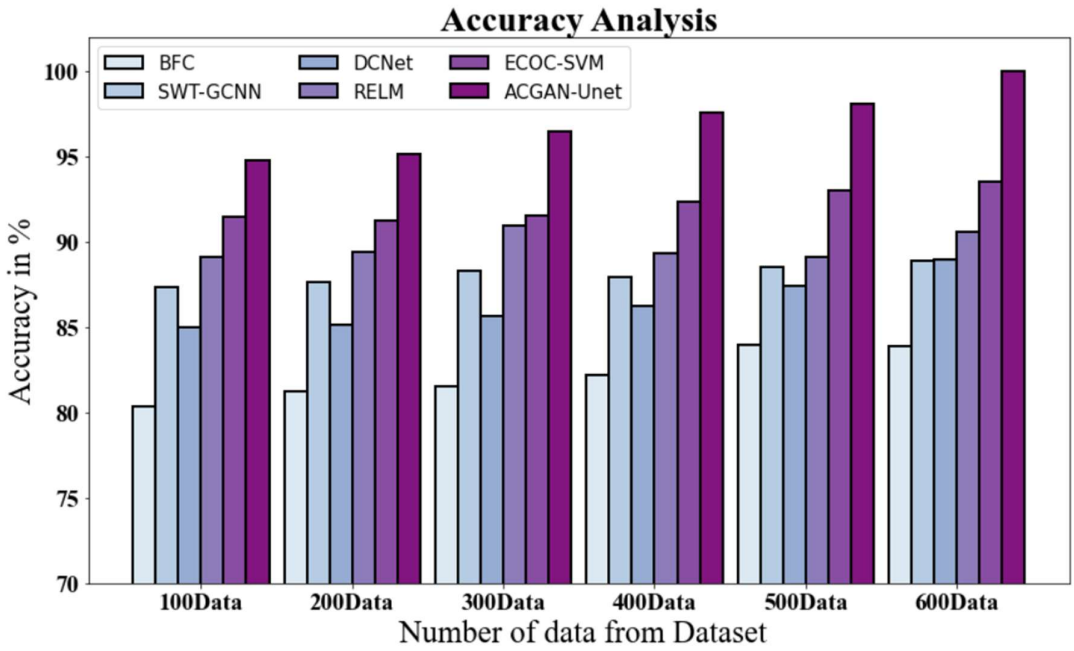

Figure 11: Accuracy Analysis for ACGAN-Unet method with the existing system

In Figure 11 and Tab. 7, the accuracy of the ACGAN-Unet approach is contrasted to that of other earlier techniques. The graph demonstrates how the machine learning approach has an improved performance with accuracy. ACGAN-Unet, for example, has accuracy of 94.765% with 100 data, while the BFC, SWT-GCNN, DCNet, RELM, and ECOC-SVM models have accuracy values of 80.345%, 87.324%, 84.987%, 89.141%, and 91.456%, respectively. However, the ACGAN-Unet model performed best with varying data sizes. Similarly, under

600 data, ACGAN-Unet has an accuracy of 99.996%, while BFC, SWT-GCNN, DCNet, RELM, and ECOC-SVM have accuracy of 83.882%, 88.928%, 88.991%, 90.564%, and 93.546%, respectively.

4.1.6. Processing Time Analysis

Table 8: ACGAN-Unet method processing time analysis with the existing system

Number of data from Dataset	BFC	SWT-GCNN	DCNet	RELM	ECOC-SVM	ACGAN-Unet
100	0.951	0.814	0.692	0.492	0.301	0.128
200	0.971	0.852	0.782	0.541	0.318	0.192
300	1.022	0.892	0.687	0.592	0.392	0.152
400	1.092	0.872	0.742	0.532	0.362	0.211
500	1.120	0.902	0.729	0.632	0.425	0.245
600	1.198	0.931	0.798	0.642	0.472	0.278

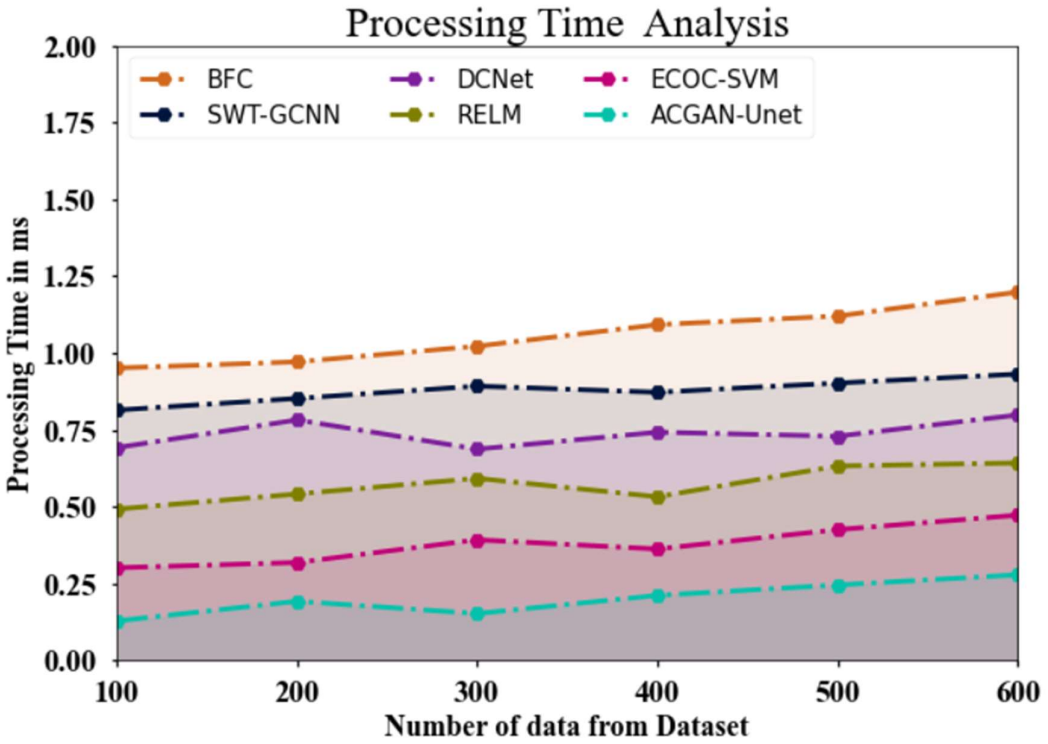

Figure 12: Processing Time Analysis for ACGAN-Unet method with the existing system

The processing time analysis of the ACGAN-Unet technique with current techniques is described in Tab.8 and Fig.12. The data clearly shows that the ACGAN-Unet method performed better than the other methods in every respect. For instance, the ACGAN-Unet technique has processed 100 data in 0.128ms while the BFC, SWT-GCNN, DCNet, RELM, and ECOC-SVM which took 0.951ms, 0.814ms, 0.692ms, 0.492ms, and 0.301ms, respectively

to process. Similarly, the ACGAN-Unet method processes 600 data in 0.278 milliseconds, while BFC, SWT-GCNN, DCNet, RELM, and ECOC-SVM methods have taken 1.198ms, 0.931ms, 0.798ms, 0.642 ms and 0.471ms respectively to process.

4.1.7. Training and Validation Accuracy Analysis

Table 9: Training and Validation Accuracy Analysis

Epochs	Training set	validation set
2	0.66	0.76
4	0.75	0.85
6	0.78	0.87
8	0.80	0.89
10	0.82	0.90
12	0.85	0.85
14	0.87	0.97
16	0.89	0.86

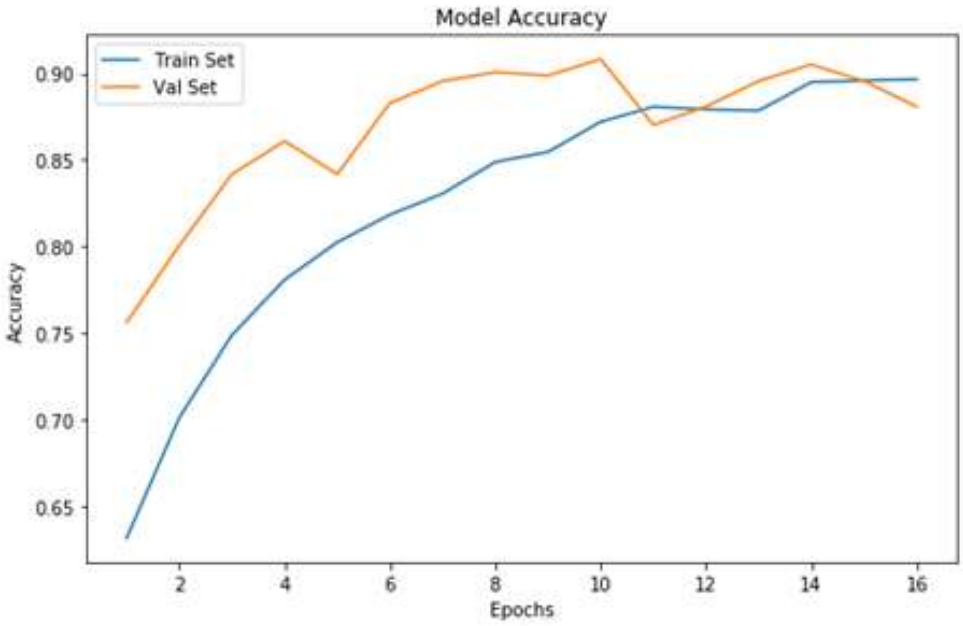

Figure 13: Training and Validation Accuracy Analysis

Tab.9 and Fig.13 describe the Model's Accuracy Analysis for the ACGAN-Unet method with existing systems. According to the data, the proposed ACGAN-Unet method performed well in all aspects. With two epochs, the ACGAN-Unet Model's training and validation accuracy is 0.66 and 0.76, respectively. Similarly, the ACGAN-Unet training and testing validation coefficients are 0.89 and 0.86 for 16 epochs, respectively.

4.1.8. Loss Analysis

Table 10: Training and Validation Loss Analysis

Epochs	Training set	validation set
2	3.7	2.6
4	1.7	1.6
6	1.6	1.4
8	1.4	1.3
10	1.2	1.1
12	1.0	1.0
14	0.9	1.4
16	0.7	1.5

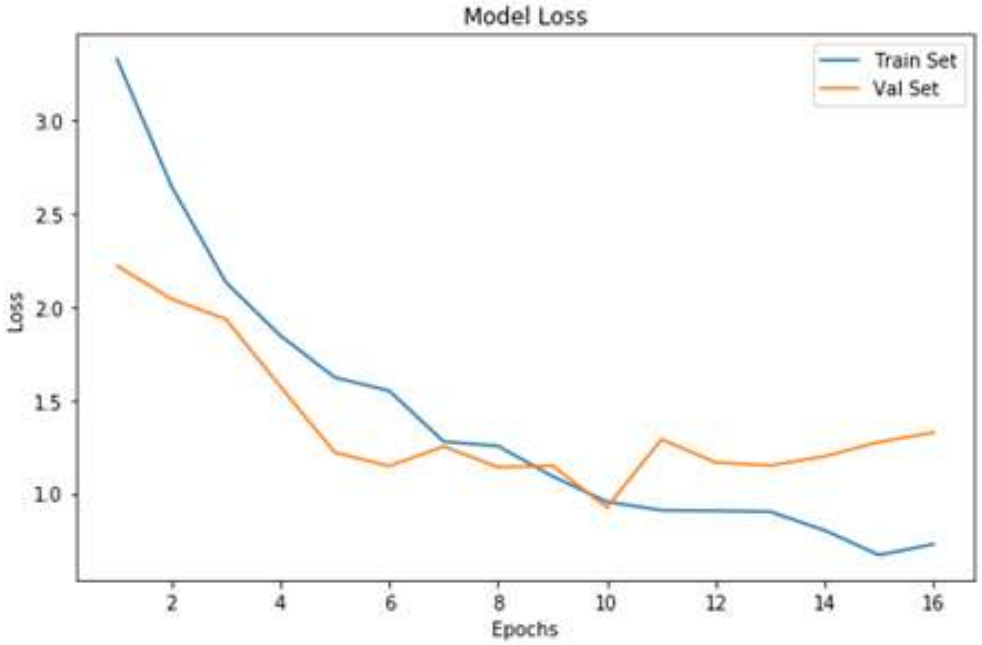

Figure 14: Loss Analysis

Tab.10 and Fig.14 describe the Model's Loss Analysis for the ACGAN-U-Net method with existing systems. According to the data, the proposed ACGAN-U-Net method performed well in all aspects. With two epochs, the ACGAN-U-Net Model loss is 3.7 and 2.6, respectively. Similarly, the ACGAN-U-Net training and testing validation coefficients are 0.7 and 1.5 for 16 epochs, respectively.

5. Conclusion

The segmentation and classification of brain tumours can be accomplished precisely and successfully using the proposed method in this paper, which applies Auxiliary Classifier

Generative Adversarial Networks (ACGAN) and a U-Net architecture. The features in MRI images are extracted using U-Net architecture, and the different types of tumours are classified using ACGAN architecture using the extracted features. According to this study, brain tumors can be categorized and identified from MRI data using Auxiliary Classifier Generative Adversarial Networks (ACGAN) with a U-Net-based architecture. The suggested model was trained using a massive amount of data from MRI pictures, both in tumor and non-tumor images, and can produce synthetic tumor images comparable to authentic tumor images. Using the generated photos enhances the model's tumor identification and classification abilities. Before the ACGAN-U-Net classifier divides tumor regions in MRI scans into the three types of tumors—glioma, meningioma, and pituitary—tumor regions are correctly separated using U-Net-based architecture. With an overall accuracy of 99.996% in determining whether a user will belong to a specific group, the proposed model outperformed existing techniques such as Bayesian fuzzy clustering (BFC), Stationary Wavelet Transform-Growing Convolutional Neural Network (SWT-GCN), Diverse capsule networks (DCNet), Regularized Extreme Learning Machine (RELM), Error-correcting output codes support vector machine (ECOC-SVM). This method can help locate and recognize malignancies fast. In the future, we intend to use Squeeze-Net and other ACGAN models, the ACGAN method, and fine-tuning techniques to classify the kind of tumor brain from MRI brain imageries.

References

1. Zhao, L.; Jia, K. Multiscale CNNs for brain tumors segmentation and diagnosis. Comput. Math. Methods Med. 2016, 2016, 8356294
2. Shree, N.V.; Kumar, T.N. Identification and classification of BTMRI images with feature extraction using DWT and probabilistic neural network. Brain Inform. 2018, 5, 23–30.
3. Louis, D.N.; Perry, A.; Reifenberger, G.; Von Deimling, A.; Figarella-Branger, D.; Cavenee, W.K.; Ohgaki, H.; Wiestler, O.D.; Kleihues, P.; Ellison, D.W. The 2016 World Health Organization classification of tumors of the central nervous system: A summary. Acta Neuropathol. 2016, 132, 803–820.
4. Chahal, P.K.; Pandey, S.; Goel, S. A survey on brain tumors detection techniques for MR images. Multimed. Tools Appl. 2020, 79, 21771–21814.
5. Sajjad, M.; Khan, S.; Muhammad, K.; Wu, W.; Ullah, A.; Baik, S.W. Multi-grade brain tumors classification using deep CNN with extensive data augmentation. J. Comput. Sci. 2019, 30, 174–182.

6. Rehman, A.; Naz, S.; Razzak, M.I.; Akram, F.; Imran, M. A deep learning-based framework for automatic brain tumors classification using transfer learning. Circuits Syst. Signal Process. 2020, 39, 757–775.
7. G. Litjens, T. Kooi, B. E. Bejnordi et al., "A survey on deep learning in medical image analysis," Medical Image Analysis, vol. 42, pp. 60–88, 2017.
8. R. Amin, M. A. Al Ghamdi, S. H. Almotiri, and M. Alruily, "Healthcare techniques through deep learning: issues, challenges and opportunities," IEEE Access, vol. 9, Article ID 98523, 2021.
9. Mehrotra R, Ansari MA, Agrawal R, Anand RS (2020) A Transfer learning approach for AI-based classification of brain tumors. Mach Learn Appl 2(9):1–12. https://doi.org/10.1016/j.mlwa. 2020.100003
10. Ayadi W, Elhamzi W, Charfi I, Atri M (2021) Deep CNN for brain tumor classification. Neural Process Lett 53(1):671–700. https:// doi.org/10.1007/s11063-020-10398-2
11. Khan HA, Jue W, Mushtaq M, Mushtaq MU (2020) Brain tumor classification in MRI image using convolutional neural network. Math Biosci Eng 17(5):6203–6216. https://doi.org/10.3934/ MBE.2020328
12. Phaye SS, Sikka A, Dhall A, Bathula D. Dense and diverse capsule networks: making the capsules learn better. arXiv:1805.04001. 2018 May 10.
13. Abd-Ellah MK, Awad AI, Khalaf AAM, Hamed HFA. Two-phase multi-model automatic brain tumour diagnosis system from magnetic resonance images using convolutional neural networks. EURASIP J Image Video Process. 2018;2018(1):97
14. Paul JS, Plassard AJ, Landman BA, Fabbri D. Deep learning for brain tumor classifcation. In: Paper presented at the Medical Imaging 2017: Biomedical Applications in Molecular, Structural, and Functional Imaging. 2017
15. Gumaei A, Hassan MM, Hassan MR, Alelaiwi A, Fortino G. A Hybrid feature extraction method with regularized extreme learning machine for brain tumor classifcation. IEEE Access. 2019;7:36266–73.
16. Mittal M, Goyal LM, Kaur S, Kaur I, Verma A, Jude HD. Deep learning based enhanced tumor segmentation approach for MR brain images. Appl Soft Comput. 2019;78:346–54.
17. P. M. Siva Raja and A. V. rani, "Brain tumor classification using a hybrid deep autoencoder with Bayesian fuzzy clustering-based segmentation approach," Biocybernetics and Biomedical Engineering, vol. 40, no. 1, pp. 440–453, 2020.

18. P. Afshar, K. N. Plataniotis, and A. Mohammadi, "Capsule networks for brain tumor classification based on mri images and coarse tumor boundaries," in Proceedings of the IEEE International Conference on Acoustics, Speech and Signal Processing (ICASSP), pp. 1368–1372, Brighton, UK, May, 2019

19. A. Arı, O. F. Alcin, and D. Hanbay, "Brain MR image classification based on deep features by using extreme learning machines," Biomedical Journal of Scientific and Technical Research, vol. 25, no. 3, 2020

20. H. Mzoughi, I. Njeh, A. Wali et al., "Deep multi-scale 3D convolutional neural network (CNN) for MRI gliomas brain tumor classification," Journal of Digital Imaging, vol. 33, no. 4, pp. 903–915, 2020.

21. Badža MM, Barjaktarović MČ. Classification of brain tumors from MRI images using a convolutional neural network. Appl Sci. 2020;10(6):1999.

22. Rehman A, Naz S, Razzak MI, Akram F, Imran M. A deep learning-based framework for automatic brain tumors classifcation using transfer learning. Circuits Syst Signal Process. 2020;39(2):757–75

23. Pashaei A, Sajedi H, Jazayeri N. Brain tumor classifcation via convolutional neural network and extreme learning machines. In: 2018 8th international conference on computer and knowledge engineering (ICCKE). IEEE; 2018 Oct 25. p. 314–9.

24. BT. DataSet. Available online: https://figshare.com/articles/dataset/brain_tumor_dataset/1512427

25. Walsh, J., Othmani, A., Jain, M., & Dev, S. (2022). Using U-Net network for efficient brain tumor segmentation in MRI images. *Healthcare Analytics*, *2*, 100098.

26. Z. Zhou, M.M.R. Siddiquee, N. Tajbakhsh, J. Liang, Unet++: A nested u-net architecture for medical image segmentation, in: Deep Learning in Medical Image Analysis and Multimodal Learning for Clinical Decision Support, Springer, 2018, pp. 3–11.

27. S. Batra, H. Wang, A. Nag, P. Brodeur, M. Checkley, A. Klinkert, S. Dev, DMCNet: Diversified model combination network for understanding engagement from video screengrabs, Syst. Soft Comput. 4 (2022) 200039.

28. Fan, Kui, Peng Peng, Hongping Zhou, Lulu Wang, and Zhongyi Guo. "Real-time high-performance laser welding defect detection by combining acgan-based data enhancement and multi-model fusion." *Sensors* 21, no. 21 (2021): 7304.